GAP JUNCTION STRUCTURES

I. Correlated Electron Microscopy and X-Ray Diffraction

D. L. D. CASPAR, D. A. GOODENOUGH, LEE MAKOWSKI, and W. C. PHILLIPS

From the Rosenstiel Basic Medical Sciences Research Center, Brandeis University, Waltham, Massachusetts 02154, and the Department of Anatomy, Harvard Medical School, Boston, Massachusetts 02115

ABSTRACT

X-ray crystallographic methods and electron microscope image analysis have been used to correlate the structure and the chemical composition of gap junction plaques isolated intact from mouse liver. The requirement that the interpretations of X-ray, electron microscope, and chemical measurements be consistent reduces the uncertainties inherent in the separate observations and leads to a unified picture of the gap junction structures. Gap junctions are built up of units called connexons that are hexagonally arrayed in the pair of connected cell membranes. X-ray diffraction and electron microscope measurements show that the lattice constant of this array varies from about 80 to 90 Å. Analysis of electron micrographs of negatively stained gap junctions shows that there is significant short range disorder in the junction lattice, even though the long range order of the array is remarkably regular. Analysis of the disorder provides information about the nature of the intermolecular forces that hold the array together.

Gap junctions are built up of units hexagonally arrayed with two-dimensional crystal-like regularity in the plane of the pair of connected cell membranes (22, 23). The unit of the 80–100 Å period lattice has been named a "connexon" (12). Connexons appear to span the bilayers of the membrane pair and the gap between them, providing the connection for intercellular communication (5).

Gap junctions have been isolated from mouse livers by treatments which solubilize most of the cell membrane but which leave the differentiated junctional domains intact (11, 12, 13). Yields of about a tenth of a milligram are obtained, starting with the livers of a hundred mice (11). These purified gap junction specimens are suitable for X-ray diffraction and chemical analysis. Determination of the X-ray scattering density map and the chemical composition could define the molecular nature of the morphological features seen in electron micrographs of purified junctions. Isolation and purification produce structural modification. Deductions about the molecular structure of isolated gap junctions can be related to the junction structure in intact cells by comparison of the morphology seen in whole tissue and in purified specimens.

Figure 1 schematically illustrates the arrangement of the connexon units in the gap junction inferred from a variety of electron microscope observations. In thin sections the junction appears as a pair of plasma membranes, each about 50–60 Å thick, separated by a "gap" 20–30 Å wide (22). With colloidal lanthanum to delineate the extracellular space, Revel and Karnovsky (22) obtained clear images of the hexagonal lattice of units in the gap. The lattice had first been seen in grazing sections of positively stained junctions in

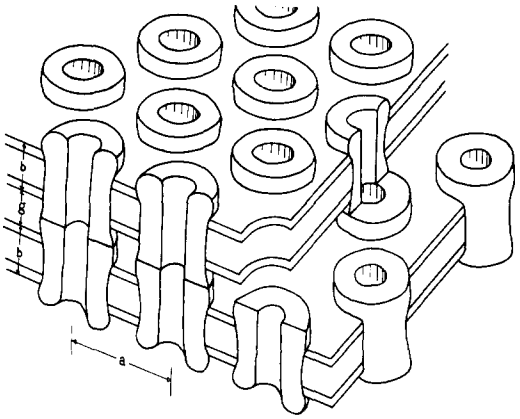

FIGURE 1 A schematic drawing of gap junction structure as deduced from a variety of electron microscope observations. The gap junction consists of a hexagonal array of units with lattice constant a. The units connect a pair of cells by spanning the two membrane bilayers, b, and the intervening gap, g. Splitting the junction through the middle of the gap leaves a hexagonal array of units in each of the separated membranes (14). The unit of the hexagonal lattice in one membrane is called a connexon (12). Bonding of the connexons in symmetric pairs at the center of the gap forms the junction structure. A channel seen as a dense core by negative straining appears to extend along the center of the pair of connexons (13, 15, 20). The lattice constant, a, of the hexagonal array is the average distance between neighboring connexons in the surface. This distance is typically 80–100 Å as measured from electron micrographs of negatively stained or freeze-fractured mouse liver gap junctions (15). The width of the gap, g, measured in thin sections as the distance between the stained membrane surfaces is in the range of 20–30 Å; the bilayer thickness, b, measured across the pair of dense lines of the individual membrane units is 50–60 Å, and the overall thickness across the junction is about 150 Å (15).

the Mauthner cell synapses by Robertson (23). The junctional lattice has also been visualized by negative stain (2, 3, 4, 15) and freeze-fracture (15). The average center-to-center spacing, or lattice constant, for the hexagonal array of connexon units as visualized by thin sectioning, negative staining and freeze-fracture is generally in the range 80–100 Å. Preliminary X-ray diffraction studies of a purified mouse liver gap junction preparation showed an hexagonal lattice with an 86 Å repeat period (16).

Among different specimens observed in the electron microscope there is considerable variation in the lattice constant and the disorder in the connexon packing. Mouse and rat liver gap junctions are large, stable and well ordered compared to those from many other tissues, which makes them favored for structural studies. Lateral dimensions are as large as 1 μm, and much of the junction seen by negative staining may consist of a single hexagonal lattice domain. Lattice constants measured for mouse liver gap junctions do, however, vary significantly. Benedetti and Emmelot (3) reported a range of 80–90 Å for the lattice constant of negatively stained, isolated gap junctions. This was reduced to 70 Å by papain digestion (4). Revel and Karnovsky (22) measured lattice constants of 90–100 Å in thin sections of tissue stained with colloidal lanthanum. Goodenough and Revel (15) recorded distances of 90–100 Å between particles for freeze-fractured mouse liver. On the P-face (protoplasmic side) the particle arrangement is usually disordered, but on the E-face (external side) the lattice of pits often has long-range regularity like the hexagonal arrays seen in negative stain.

The diameter of the portion of the connexon unit extending across the gap as measured by negative staining of isolated junctions is about 60 Å. Negative staining also shows a stain-penetrable core about 20 Å in diameter in the center of the connexons. Edge-on views of the junction which have been obtained in negative stain indicate that the stain-filled core extends across both membranes and the intervening gap (13).

Particles seen on the P-face of freeze-fractured junctions correspond to the portion of the connexon extending across the membrane bilayer. The ratio of the diameter of these particles to their separation is similar to that measured by negative staining, but it is difficult to obtain accurate particle dimensions from the metal-shadowed replicas. Striations have been observed in the protoplasmic surface of the junction by freeze-drying and by freeze-etching, suggesting some protrusion of the connexon into the cytoplasm (12). Freeze-etching of split junctions reveals the ends of the connexons protruding from the external surface of the membrane that correspond to the portions seen by negative staining in the gap of connected junctions (14).

The thickness of the junction measured in thin sections is about 150 Å (15). In centrifuge pellets of purified junctions the closest stacking distance is also about 150 Å. This dimension corresponds to the length of a pair of connexons spanning the junction.

The connexon unit pictured from these electron microscope observations (Fig. 1) is a hollow cylin-

der about 75 Å long, 60 Å outside diameter and 20 Å inside diameter. This is a very approximate representation, but it suggests how much space may be occupied by the protein presumed to form the connexon. SDS-gel patterns from purified junctions have been interpreted to indicate that the connexon is composed of one principal protein, connexin, with a mol wt about 20,000 in preparations treated with collagenase and hyaluronidase (11). Bands on SDS gels with mol wt in the range of 20–35,000 have been observed under different conditions (8, 10, 16). The connexon does appear to be an oligomer of identical subunits, but the number derived from chemical measurements of subunit molecular weight and morphological estimates of overall volume is ill defined in the range from about four to eight. Hexagonal lattice symmetry, of course, suggests an underlying sixfold molecular symmetry for the connexon.

Our schematic Fig. 1 poses questions about the junction structure which we have explored by coordination of X-ray diffraction and electron microscopy. Do the connexons really form tubes that link the protoplasms of the connected cells? Determination of the molecular structure would provide an answer to this question. Since the connexons are arranged with two-dimensional crystalline regularity in the membranes, it is possible to apply crystallographic methods to obtain an averaged picture of a connexon from diffraction patterns of junction lattices. The detail that can be seen from the diffraction patterns is limited, however, by the disorder in the structure.

Disorder is a nuisance for the crystallographic analysis, but it does appear to be intrinsic to the junction structure. In Fig. 1, no connections are indicated among the hexagonally arrayed connexons in the plane of the lipid bilayer. What sort of interactions hold the connexons together in the junction lattice? Quantitative analysis of the disorder and the variation of the lattice observed by X-ray diffraction and electron microscopy provides a way to characterize the bonding potential between connexons as a function of their separation. As we will show, within a single, well-ordered, negatively-stained lattice domain, the mean variation in the separation between neighboring connexons is generally about a third the average lattice constant; furthermore, among different junction specimens, the average lattice constant of hexagonal domains differs by more than 10%. If these variations are not artifacts induced by the preparative treatments for electron microscopy, then it appears that the energy of interaction between connexons does not change much over a broad range of separations. Nevertheless, the linkages among the connexons are strong enough to maintain the hexagonal lattice even when the rest of the membrane (of which the junction is a part) is disrupted.

Artifacts in the structures seen in the electron microscope can be assessed by comparison with the X-ray diffraction patterns from the specimens before dehydration, staining, freezing, or other preparative treatments for electron microscopy. Lattice dimensions and disorder can be measured directly by both techniques. When this comparison indicates that we are seeing the same structure with X-rays and electrons, then, as in the following paper (18), we can use the information from electron microscopy for quantitative analysis of the X-ray intensity measurements.

MATERIALS AND METHODS

Gap junctions were isolated in bulk as previously described (11). In some specimens, 0.02% trypsin (Type III, Sigma Chemical Co., St Louis, Mo.) was used in addition to the usual digestion with collagenase and hyaluronidase. This additional digestion had the effect of inducing many of the gap junctions to form closed vesicles 0.1–0.5 μm in diameter (13) as well as removing nonjunctional material from the final pellet.

Fixation in aldehydes and osmium tetroxide was carried out as reported previously (15). Specimens for thin section were routinely stained in block with 1% aqueous uranyl acetate after osmium tetroxide fixation and a distilled water rinse. Freeze-fracturing was done on a Balzers BA360M or BAF301 (Balzers AG, Balzers, Liechtenstein) according to standard techniques. In order to correlate electron microscope and X-ray diffraction data, a small piece from the edge of each X-ray specimen was used to cut thin sections for electron microscopy. The purity of the specimen and the degree of order produced by centrifugation could be judged from the thin sections.

Optical diffraction from electron micrographs of negatively stained gap junctions was used to locate highly ordered regions of junction lattice. Selected areas were densitometered on a 25-μm grid with an Optronics rotating-drum microdensitometer (Optronics International, Inc., Chelmsford, Mass.). Two-dimensional Fourier transforms were calculated, and the intensity and phase of the diffraction peaks in the transform of the hexagonal lattice were used to recalculate a filtered image. When necessary, the phases were corrected for the effect of the phase-contrast transfer function (9).

To prepare specimens for X-ray diffraction, isolated junctions were centrifuged into a pellet at 250,000 *g* for about 2 h, using BEEM hemihyperboloid polyethylene

capsules (Cat. no. 2323, Ladd Research Industries, Inc., Burlington, Vt.) in Epon centrifuge adapters (12). The centrifuged pellets were either fixed with 0.25% gluteraldehyde or left unfixed. The pellets were placed in thin-walled, flattened quartz capillaries and sealed with wax to prevent dehydration. The specimens were usually oriented in the capillaries so that the X-ray beam passes through the pellet normal to the direction of the centrifugal field.

X-ray studies were carried out using CuKα radiation from an Elliott rotating anode generator (Marconi-Elliott Avionic Systems, Ltd., Borehamwood, Herts, England), with a 0.1 × 1.0-mm focal spot source. Diffraction patterns were recorded on Ilford Industrial G film (Ilford Ltd., Ilford, Essex, England) with cameras employing either a bent quartz crystal monochromator, two bent totally reflecting mirrors or a quartz monochromator and one mirror. Sample-to-film distances were generally between 8 and 13 cm, although a few patterns were recorded with a 31-cm specimen-to-film distance. The dimensions of the focused beam at the film were generally small enough to give order-to-order resolution of at least 1,000 Å, which is finer than the detail in the pattern determined by the 150 Å junction thickness. Exposure times were usually between 1 and 4 days. The optical densities on the films were measured with an Optronics rotating-drum microdensitometer.

The nitrogen and phosphorous content of purified gap junctions were determined by Galbraith Laboratories (Knoxville, Tenn.). Isolated, lyophilized gap junctions were sealed under nitrogen in glass ampules for shipment. Material from 300 mouse livers was used for each measurement, and three measurements were made.

Continuous sucrose gradients were generated in Beckman SW41 tubes (Beckman Instruments, Inc., Palo Alto, Calif.) with d = 1.126 and d = 1.277 as the limiting sucrose densities. 1–2 milliliter aliquots of a concentrated junction suspension were then layered on top of the gradients. The tubes were centrifuged at 280,000 g for 24 h at 4°C, punctured at the bottom, and collected in 0.5-ml aliquots. Absorption at 280 nm was measured for each aliquot after dilution to 1.0 milliliter with distilled water. Sucrose concentration was measured by refractometry of parallel gradients.

RESULTS

Electron Microscopy

NEGATIVE STAIN: Several crystalline domains are often visible in a micrograph of a negatively stained, isolated gap junction plaque. In each domain the connexons lie approximately on a hexagonal lattice. Connexons are displaced slightly from the positions they would occupy in a perfect hexagonal lattice. This short range disorder is usually large enough to be readily visible in micrographs of negatively stained specimens. However, averaged over many unit cells, the lattices are often quite accurately hexagonal.

Disorder in the junction lattices can be analyzed quantitatively by optical diffraction. The number of diffraction orders visible in an optical diffraction pattern depends on the degree of short-range disorder in the lattice. More crystalline reflections are visible in diffraction patterns from well-ordered lattices. The sharpness of the crystalline reflections provides a measure of the long-range order. Crystal domains which are accurately hexagonal averaged over a large number of repeats will give rise to sharp crystalline reflections, even when there is significant short range disorder.

Figure 2 shows an analysis of a high-contrast, underfocused image of a very well-ordered, isolated gap junction taken by N. B. Gilula (The Rockeller University, New York). This junction was chosen for analysis because its lattice is much better ordered than most junction lattices observed. Fig. 2*b* is a high magnification view of a very well-ordered crystalline domain from the junction shown in Fig. 2*a*. Its optical diffraction pattern is shown in Fig. 2*c*.

The crystalline reflections from a two-dimensional hexagonal lattice are indexed according to their direction and distance from the center of the pattern. The two principal directions are chosen to be at an angle of 60° to one another. The first reflection directly below the center of the optical diffraction pattern in Fig. 2*c* is indexed as the (1,0). The strongest reflections in this pattern are the (1,0), (1,1), and (2,0) and their symmetrically equivalent reflections about the origin. These three reflections are the only ones observed in optical diffraction from many gap junction specimens. The junction lattice shown in Fig. 2 is better ordered than is commonly observed, and the reflections in the optical diffraction pattern extend out to the (4,0) reflection.

The magnitude of the short-range disorder in the lattice can be estimated from the spacing of the highest index hexagonal lattice reflections observed in the optical diffraction pattern. For the pattern in Fig. 2*c*, this is the 18 Å spacing of the (4,0) reflection which provides a measure of the mean displacement of the connexons from the points of a perfect lattice. Lattices whose diffraction patterns fade out closer to the center have correspondingly larger short-range disorder.

FILTERED IMAGES: The relative intensities of the hexagonal lattice reflections in the optical diffraction pattern contain information about the

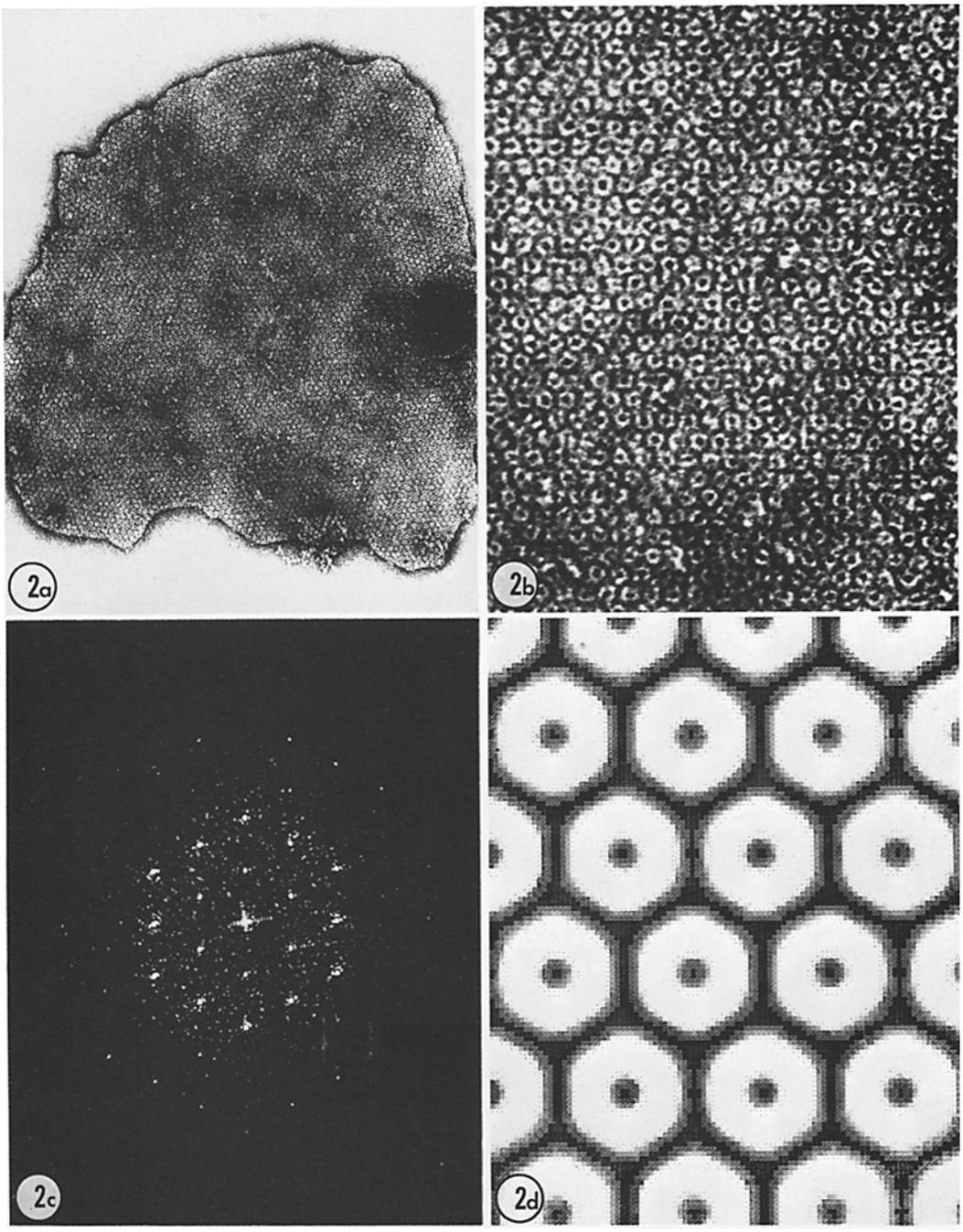

FIGURE 2 Micrograph of a negatively stained, isolated gap junction. (*a*) Low magnification view (× 90,000) of an isolated junction plaque about 0.7 μm across with hexagonal lattice extending throughout the plaque. Higher magnification view (× 310,000) of this junction (*b*) shows that hexagonal packing of the units is highly ordered with a lattice constant of about 85 Å. Its optical diffraction pattern (*c*) extends out to the fourth order (4, 0) reflection which falls at a spacing of 18 Å. Calculation of a filtered image of the junction (*d*) from the micrograph shows the average distribution of stain about the connexons.

average structure of the connexons in the micrograph. This information may be distorted by the focusing of the electron microscope (9). These distortions can be corrected during the computer filtering of a micrograph. Fig. 2*d* is a filtered image computed from the junction shown in Fig. 2*a*. The filtered image is equivalent to a superposition image of the connexons in the lattice, assuming that they all lie exactly on a hexagonal lattice. Because each connexon has suffered some small random displacement from its ideal lattice location, the filtered image is an imperfect superposition of the connexons. Thus, the short-range disorder smears the features of the filtered image, and preserves only those which have dimensions larger than the average displacement of the connexons from their ideal lattice positions.

In the filtered image, the connexons appear cylindrically symmetric because the extent of the short-range disorder is greater than the lateral dimensions of any fine detail in the negatively stained connexons. Only the densely staining central core is large enough to stand out as a significant feature of the connexon substructure in the average image. The other details which can be observed on individual connexons in the micrographs are not consistently reproduced in all the units of the lattice. Comparison of filtered images from several micrographs shows that the relative density of stain accumulating at the centers of the connexons and between the units is variable. Filtered images of two other gap junction specimens are shown in Fig. 3. Greater stain accumulation has occurred on the threefold axis in the array shown in Fig. 3*a*, whereas in Fig. 3*b* the units are more heavily stained in their centers. This is in contrast to the lattice in Fig. 2*d* in which stain accumulation in the centers of the connexons and between the units is about the same. The lattice constant of the array shown in Fig. 3*b* appeared to be 2–3% less than that for the junction shown in Fig. 3*a*.

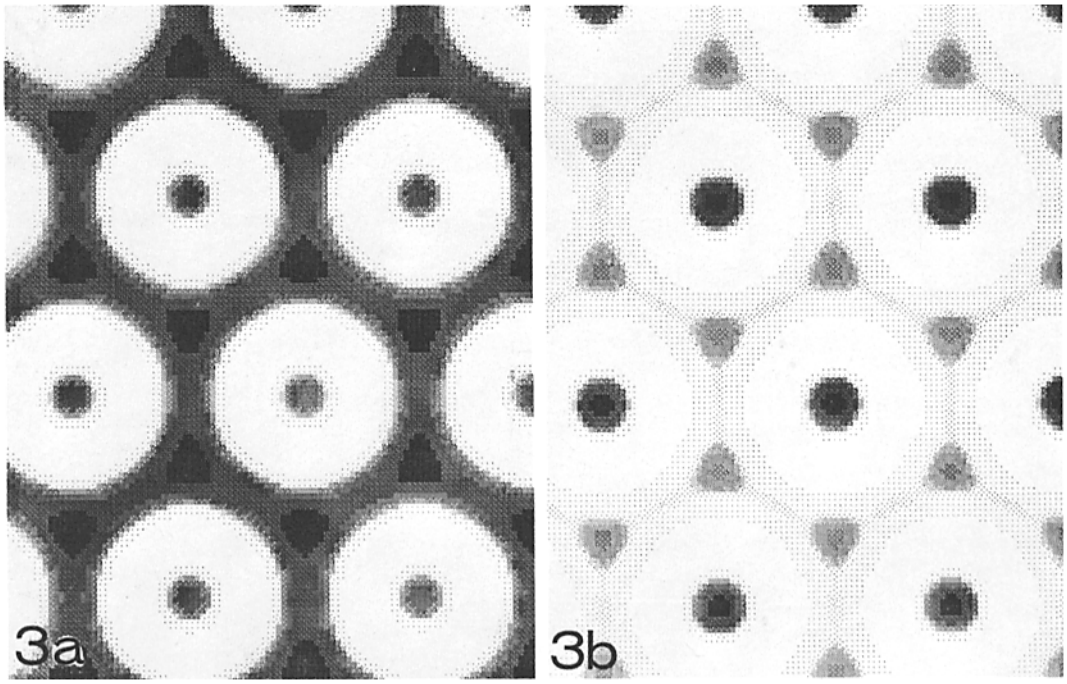

FIGURE 3 Computer-filtered images of negatively stained, isolated gap junctions. These two images were chosen to show the range of variation in the stain distribution. The junction shown in Fig. 3*a* stained much more densely between units than in the center of the connexons. Stain accumulation was much greater in the center of the connexons in the lattice shown in Fig. 3*b*. The lattice constants of the junctions shown in 3*a* and 3*b* are about 89Å and 86Å, respectively. In the display, the calculated densities were scaled so that the minimum density calculated was set to the lightest level on the grey scale and the maximum density was set to the darkest level on the grey scale. Only information about the relative stain distribution among different parts of the structure is contained in these images.

LATTICE DISORDER: Figure 4 illustrates an analysis of the disorder in the junction lattice directly from the micrograph. Figure 4*a* is an enlargement of another section of the micrograph in Fig. 2*a* with the centers of the connexons marked. Fig. 4*b* is a reproduction of the dots marking the positions of the centers of the connexons with a hexagonal lattice drawn to fit as closely as possible the marked centers. Two crystalline domains separated by a grain boundary are evident. Two local lattice defects are apparent in the larger crystalline domain. Within the larger lattice domain, the average packing is quite accurately hexagonal as demonstrated by the extent to which the lattice lines which have been drawn remain straight and equally spaced over most of the domain. The high degree of long-range order often found in gap junction lattices is remarkable, considering the magnitude of short-range disorder observed in these specimens. The short-range disorder may be seen by observing the deviation of the dots indicating the centers of the connexons from the intersections of the lattice lines.

The disorder can be further characterized by optical diffraction. Figure 5*a* and *b* show the pattern of connexon positions and its optical transform. Two sets of lattice reflections result from the presence of two crystalline domains at slightly different orientations. The smaller domain gives rise to reflections at a slightly smaller radius, indicating a larger lattice constant. The intensity of these reflections damps out more quickly with increasing radius than that of the reflections from the larger domain, due to the greater short-range disorder in this portion of the lattice.

FREEZE-FRACTURE: The order in the junction lattice has also been examined in freeze-fractured specimens. Freeze-fractured whole mouse liver gap junctions exhibit a characteristic pattern of particles on the P-face (protoplasmic side) and pits on the E-face (external side). The array of particles on the P-face is relatively disordered under most circumstances, often appearing to have liquid-like packing rather than a packing which can be identified as a disordered lattice. The lattice of pits on the E-face more closely resembles the hexagonal packing observed in negatively stained junctions. Under conditions which uncouple the junctions, the lattice order observed in freeze-fractured specimens may be significantly improved.

As reported by Goodenough and Gilula (14), perfusion of mouse livers with 0.5 M sucrose before fixation leads to increased order in the gap junction lattices visualized by freeze-fracturing. Figure 6 shows a freeze-fractured junction from a mouse liver perfused with 0.5 M sucrose before fixation. In Fig. 6*b*, the positions of the particles and pits have been marked by dots as was done in Fig. 4*a*. This emphasizes the continuity of the lattices on the E- and P-faces. The order in the particles of the P-face is significantly more regular than that from gap junctions not subject to the sucrose treatment. The lattice, however, is not so well ordered as is generally seen in images of isolated, negatively stained gap junctions.

THIN SECTION: The order in the stacking of the junctions in centrifuge pellets can be analyzed both by electron microscopy and by X-ray diffraction. The analysis presented in this section will be compared to corresponding results from X-ray diffraction data derived in the following paper (18). Electron micrographs of thin sections of the pellets prepared for X-ray diffraction in cross section are shown in Figs. 7 and 8. Figure 7*a* is from a relatively well-oriented sample. Figure 7*b* which shows close contacts between some junctions is from a more typical X-ray specimen corresponding to the diffraction pattern in Fig. 10*a*. Figure 8*a* shows a thin section from a partially dried specimen, F68A. An X-ray diffraction pattern from this specimen is shown in Fig. 11*c*. The orientation is somewhat improved by the partial drying, and the stacking of the junctions in the pellet is also enhanced. Figure 8*b* shows vesicles formed by the trypsin treatment of specimens. Orientation is very poor after centrifugation, demonstrating that the vesicles are resistant to flattening. An X-ray diffraction pattern from a trypsin-treated specimen, F38, is shown in Fig. 10*b*.

Although there does not appear to be any periodic stacking of the junctions, the occasional pairing as seen in Fig. 7*b* leads to diffraction effects which must be taken into account in the analysis of the X-ray patterns. To demonstrate the effect of this partial ordering on the diffraction patterns, tracings of the electron micrographs were drawn in which each junction was represented by a thin line at the center of the gap. A tracing and its optical diffraction pattern are shown in Fig. 9. The optical diffraction pattern exhibits distinct fringes due to the partially ordered stacking of junctions in the specimens. These interference fringes have a wavelength of about 150 Å corresponding to the distance between junctions seen in the pairing of junctions in

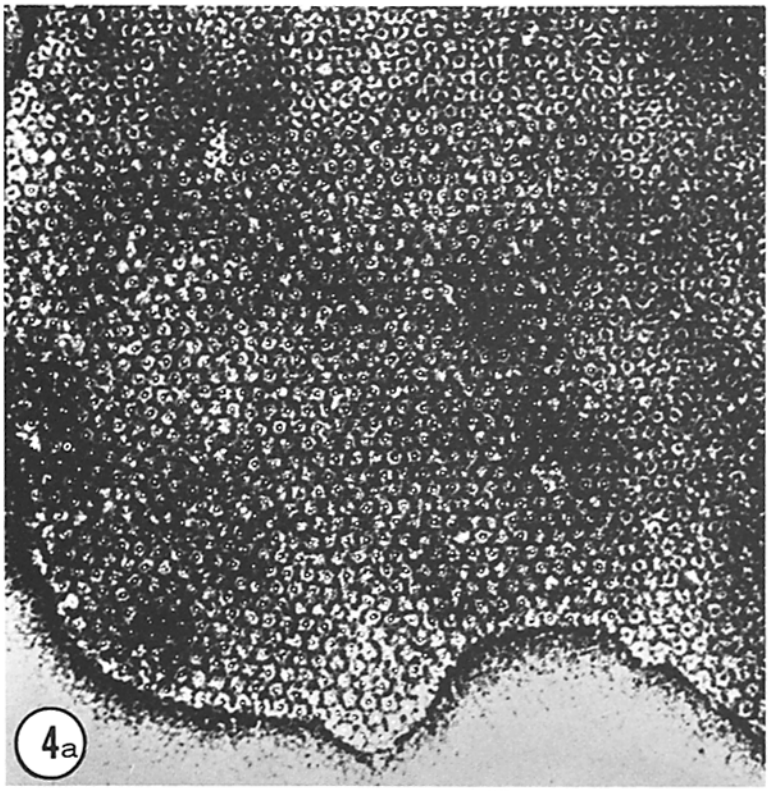
4a

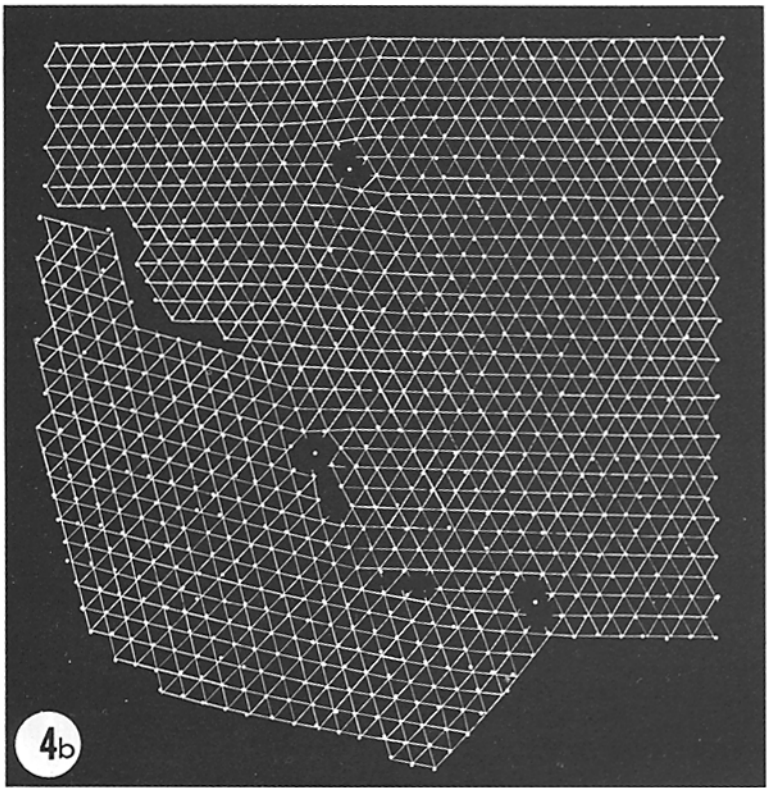
4b

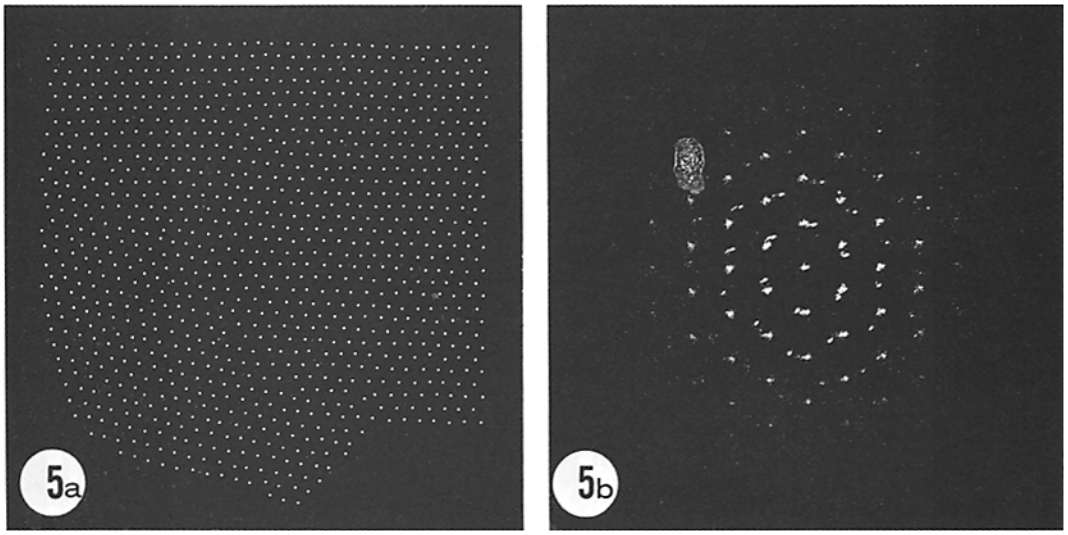

FIGURE 5 The position of the connexon centers marked as dots (*a*) for the portion of the junction shown in Fig. 4*a*, and the optical transform (*b*) of this array of dots. The optical transform provides an analysis of the order in this array which is complementary to the analysis illustrated by the drawing of lattice lines in Fig. 4*b*. The optical transform shows two hexagonal arrays of spots, the weaker of which corresponds to diffraction from the smaller lattice domain in the lower left of the junction lattice (cf. Fig. 4*b*). This portion of the lattice is rotated by about 15° relative to the larger domain in the upper right of the array. The diffraction from the smaller domain shows a slight distortion of the hexagonal form: the lattice is expanded about 3% along the vertical compared to the larger domain which has a regular hexagonal lattice. The sharpness of the spots in the diffraction from both domains reflects a high degree of long-range order. Since the sizes of the spots in (*b*) are inversely proportional to the size of the lattice domains in (*a*), the average lattices corresponding to each domain are very regular. Differences in the short-range order in the two domains are indicated by the way in which the intensity of higher-angle diffraction decreases in the two sets of spots. Diffraction spots from the smaller domain are not observed beyond the third order, whereas fourth order diffraction spots are clearly evident from the larger, more regular domain. Comparison of this diffraction pattern with the optical diffraction from the micrograph itself (Fig. 2*c*) shows that the fade-out of the higher-angle spots is very similar although the relative intensities of the spots are different. The intensity of the diffraction from the micrograph is modulated by the Fourier transform of the connexon unit, but the fade-out is determined by the short-range disorder in the packing arrangement.

the micrographs. Analysis of X-ray patterns shows that this irregular close packing of the junctions gives rise to observable modulation of the intensity of the X-ray diffraction (18).

X-ray Diffraction

We had anticipated obtaining high-resolution structural information from the X-ray diffraction

FIGURE 4 Close-up (× 280,000) view (*a*) of a portion of the junction shown in Fig. 2*a*. The centers of the connexon units as judged by eye have been marked over a part of the lattice and are shown as dots superimposed on the micrograph. These dots marking the centers of the units are reproduced in (*b*) with lattice lines drawn in at 1.2× the scale in (*a*). Straight line segments were drawn to fit rows of dots as closely as possible; the lines were kept straight as long as the displacements of dots to either side of the row were randomly distributed. The lines were curved to fit bends in the lattice arising from dislocations. Lines were terminated where there were changes in direction corresponding to grain boundaries or other defects. The drawing of the lattice lines was constrained so that the three nonparallel sets intersected at common points. These points define the best "equilibrium" position of the units in the lattice. The displacement of the dots from the intersection of the lines provides a measure of the short-range disorder. The regularity in spacing of the lines over large distances illustrates the long-range order in the lattice.

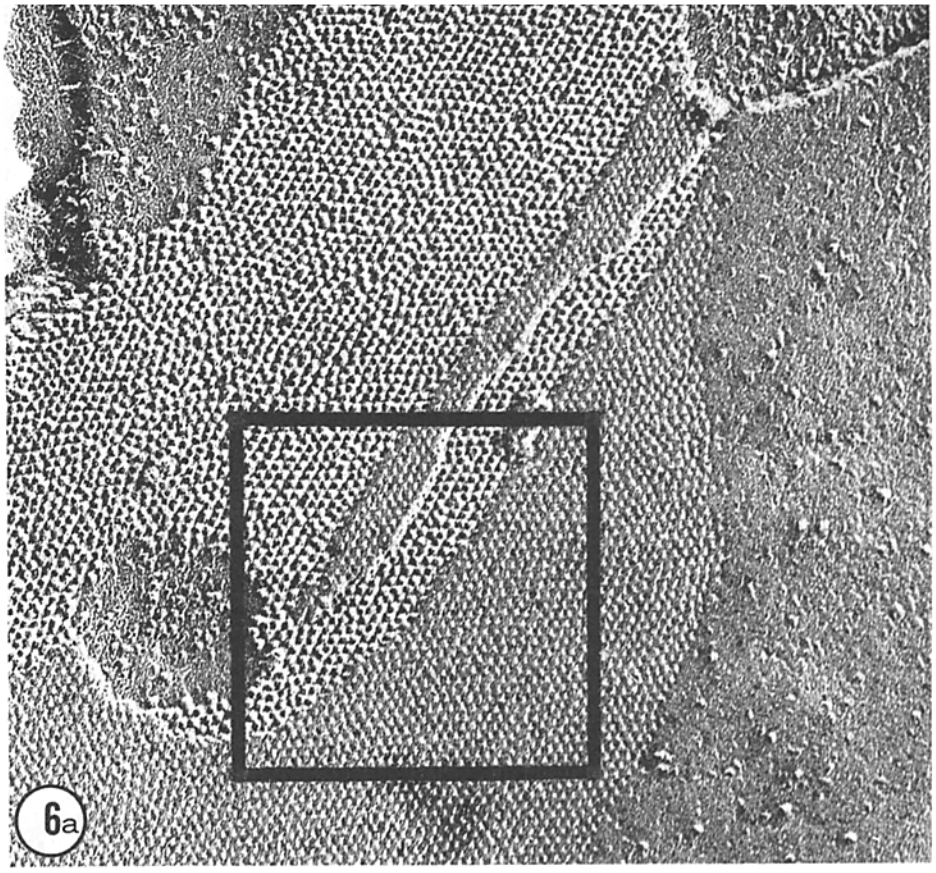

6a

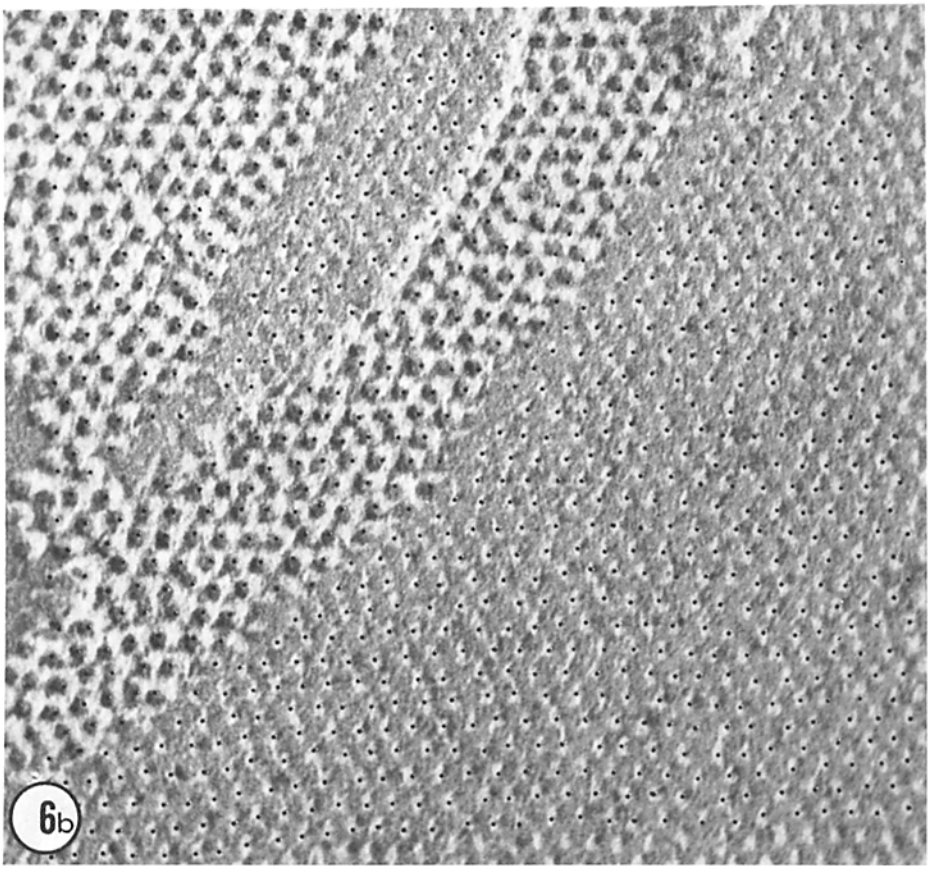

6b

patterns. However, one of the striking aspects of the X-ray patterns is that the resolution to which hexagonal lattice reflections extend is comparable to that seen in optical diffraction from the electron micrographs. Measurements have been made on X-ray diffraction patterns from over three dozen specimens, representing about half the specimens looked at. The other half of the specimens, due to disorder and/or disorientation, produced diffraction patterns which were unsuitable for any measurements. The six X-ray diffraction patterns shown in Figs. 10 and 11 have been selected to show the range of diffraction patterns obtained. Each of these is the bes. diffraction pattern obtained from a specimen treated in a particular fashion.

The X-ray diffraction photographs in Figs. 10 and 11 are oriented so that vertical corresponds to the direction perpendicular to the plane of the junction in the specimen. Strong diffraction is observed in both the meridional (vertical) and equatorial (horizontal) directions out to a spacing of about 30 Å. In the poorly oriented specimens, the diffraction is arced until the pattern has nearly circular symmetry. Even in the best oriented specimens, there is visible overlap of equator and meridian.

MERIDIONAL DIFFRACTION: The meridional diffraction is determined by the electron density distribution perpendicular to the plane of the junction. The strong diffraction out to 30 Å spacing is expected for lipid bilayers that have a characteristic high electron density contrast between the polar groups and hydrocarbon chains of the lipids. Weak diffraction is occasionally observed out to 10 Å spacing on the meridian. The partial stacking of junctions in the X-ray pellet as seen in micrographs of thin sections such as that in Fig. 7*b* should give rise to interference effects on the X-ray diffraction patterns. The interference will affect the X-ray diffraction pattern in much the same way as it did the optical diffraction pattern in Fig. 9. Thus, the continuous diffraction on the meridian may be thought of as diffraction from randomly positioned gap junctions modulated by an interference term caused by the occasional stacking of the junctions in the pellet.

Morphological and physiological data indicate that the junctions are built up from a symmetrically related pair of membranes. Centrosymmetric symmetry of the junction profile requires the transform on the meridian to be a real function. As will be discussed in the following paper (18), application of the minimum wavelength principle shows that the very sharp small-angle intensity minima between meridional diffraction fringes must be nodes of the transform. Significant variation in the positions of these nodes was observed among different specimens. These meridional variations correlate with observed shifts in lattice constant of the equatorial diffraction. In the next paper, the positions of these zeros of the transform are shown to be sensitive indicators of the width of the gap between membranes, and indicate that gap width is correlated with lattice contant over the range of variations observed.

EQUATORIAL DIFFRACTION: The equatorial diffraction is due to the electron density distribution in the plane of the membrane. Since the connexons are ordered into a hexagonal lattice, the diffraction exhibits lattice sampling. The equator of the X-ray diffraction pattern from the junction seen edge-on corresponds to a cross-sectional sampling of optical diffraction patterns from the electron micrographs of negatively stained junctions viewed face-on. Many junctions contribute to the recorded X-ray diffraction, so that the equatorial diffraction is from a circular average of the set of hexagonal lattice reflections. The equatorial arc nearest the origin in the X-ray pattern is the

FIGURE 6 A freeze-fractured gap junction from a mouse liver which has been perfused with 0.5 M sucrose before fixation. The particles on the P-face are attached to the protoplasmic half of the membrane; the pits on the E-face are in the extracellular half of the membrane bilayer. Continuity of the hexagonal lattice between the P- and E-faces is evident. The lattice in the portion of the junction outlined in (*a*) (× 160,000) has been analyzed in (*b*) (× 410,000) where the positions of the particles and pits have been marked by dots. The pattern of dots shows that the order in the two faces is similar. In contrast, the arrangement of particles generally observed in the P-face from freeze-fracture of intact tissue is much more disordered than seen here, although the pits in the E-face are often arranged in a recognizable hexagonal lattice. Compared with the lattice of the well-ordered negatively stained specimen in Fig. 4, the lattice in this freeze-fracture specimen shows greater short-range disorder.

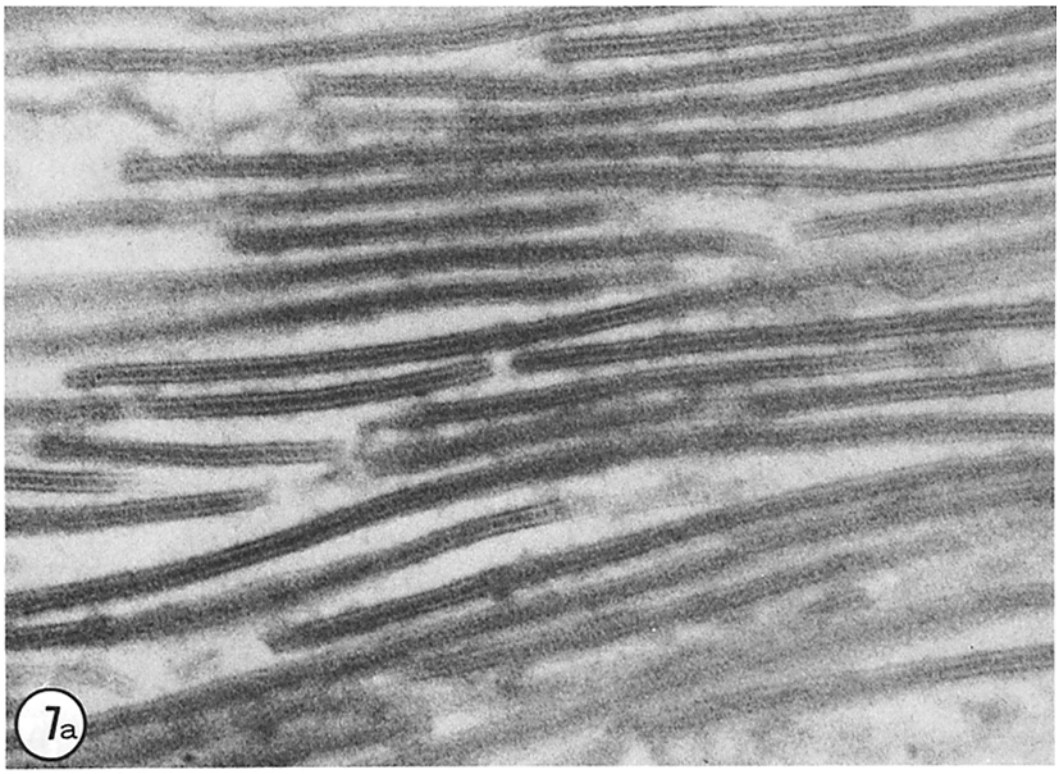
7a

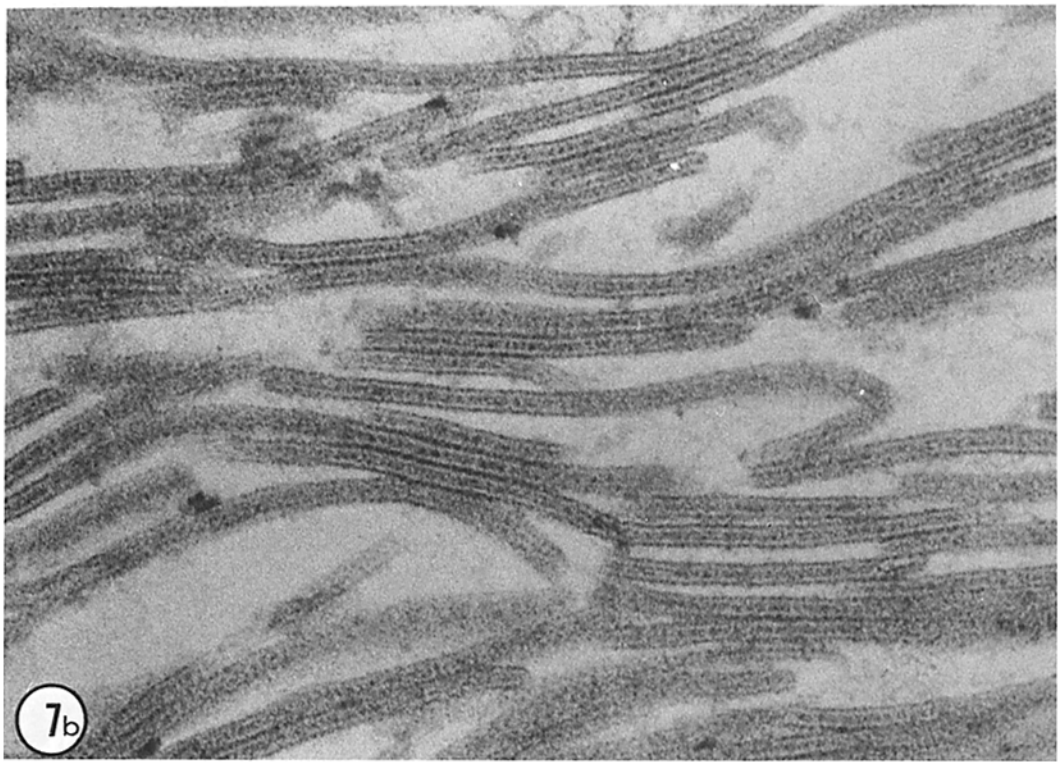
7b

(1,0) reflection which corresponds to the six spots making up a hexagon about the origin in the optical diffraction pattern in Fig. 2*c*. The twelve spots making up the next hexagonal ring of reflections in the optical diffraction pattern fall at two different radii, the (1,1) reflection being closer to the origin than the (2,0), corresponding to two closely spaced reflections in the X-ray diffraction patterns.

Measurement of the spacing of these reflections confirms that the junction lattice is hexagonal and allows accurate calculation of the lattice constant. Lattice constants range about 80-90 Å, and a few representative measurements are listed in Table I. In several specimens, pairs of hexagonal reflections were observed corresponding to two different lattice constants differing by 5-10%. Three sets of diffraction data from one specimen, F22A, were collected over a period of weeks. In each succeeding experiment the lattice constant was smaller, and the meridional zeros had shifted to larger angles. In general, the lattice sampling is weak beyond the (2,1) reflection and is replaced by a broad band of continuous diffraction centered around 10 Å spacing. In some specimens the lattice sampling extends out to the (4,0) reflection.

In patterns from the best oriented specimens, very weak off-equatorial maxima are observed which may be identified as diffraction on lattice lines extending parallel to the meridian, above and below each equatorial reflection. These lattice lines are orthogonal analogues to the layer lines seen in fiber patterns. The poor orientation of the specimens makes estimation of the magnitude of this diffraction difficult.

SPECIMEN VARIATION: Figure 9*a* is a diffraction pattern from a relatively well oriented, glutaraldehyde-fixed specimen, E153. This pattern is unique in terms of the amount of information it contains. Some specimens appear to be polydisperse. They are made up of gap junctions which differ slightly in structural detail. Polydispersity makes the patterns indistinct and damps the intensity of the higher-angle reflections, similar to the effect a temperature factor has on a crystal diffraction pattern. The very clear diffraction out to 10 Å spacing on the E153 meridian indicates that the specimen was very homogeneous. Equatorial lattice sampling extends beyond the (4, 0) reflection, indicating greater short-range order in the hexagonal lattice than is commonly observed. The preparative procedure necessary for the reproducible production of homogeneous specimens is not yet established. Most of the diffraction patterns obtained do not have the resolution of the E153 photograph. However, all the junction diffraction patterns collected have the same general form as that observed for this specimen.

Figure 10*b* shows a diffraction pattern from a trypsin-treated specimen (F38). The orientation is extremely poor due to the formation of vesicles as illustrated in the electron micrograph of a thin section from a trypsin-treated specimen in Fig. 8*b*. The equatorial reflections are very sharp, indicating an extensive, well-ordered lattice. The lattice constant for this specimen is 82.0 Å compared to 86.7 Å for E153. The positions of the nodes of the meridional diffraction from F38 and E153 are significantly different (Table I).

After specimen E153 was allowed to dry in air, the diffraction pattern, Fig. 11*a*, showed greatly increased diffuse low-angle scatter, reduced higher-angle scattering, and very little lattice sampling on the equator. Figure 11*b* was obtained from a portion of the E153 specimen to which Hg had been added. This resulted in a slight shift in the meridional zeros and an increase in the lattice constant. Figure 11*c* shows the X-ray diffraction pattern from a partially dehydrated specimen. The meridional interference is significantly greater in this specimen, but it is only clearly evident on the

FIGURE 7 Electron micrographs of thin sections of junction pellets as prepared for X-ray diffraction studies showing different packing arrangements. The pellets have been sectioned parallel to the direction of the centrifugal field. The junction plaques tend to orient with their flat surfaces normal to the direction of centrifugation. In (*a*) (× 200,000), the junctions are flat and lie more or less parallel but are separated from each other by a variable distance. This specimen is a very clean one that was prepared in buffer at pH 8.2. The specimen shown in (*b*) (× 200,000) which was centrifuged from an unbuffered suspension is more typical of those used for the X-ray diffraction studies. In (*b*), there are regions where junctions are in close contact with a center-to-center spacing of about 150 Å. The slight curvature of the junction layers in (*b*) leads to less parallel orientation than in (*a*). The ordering in the junction stacking in specimens like that shown in (*b*) is analyzed by opitcal diffraction in Fig. 9.

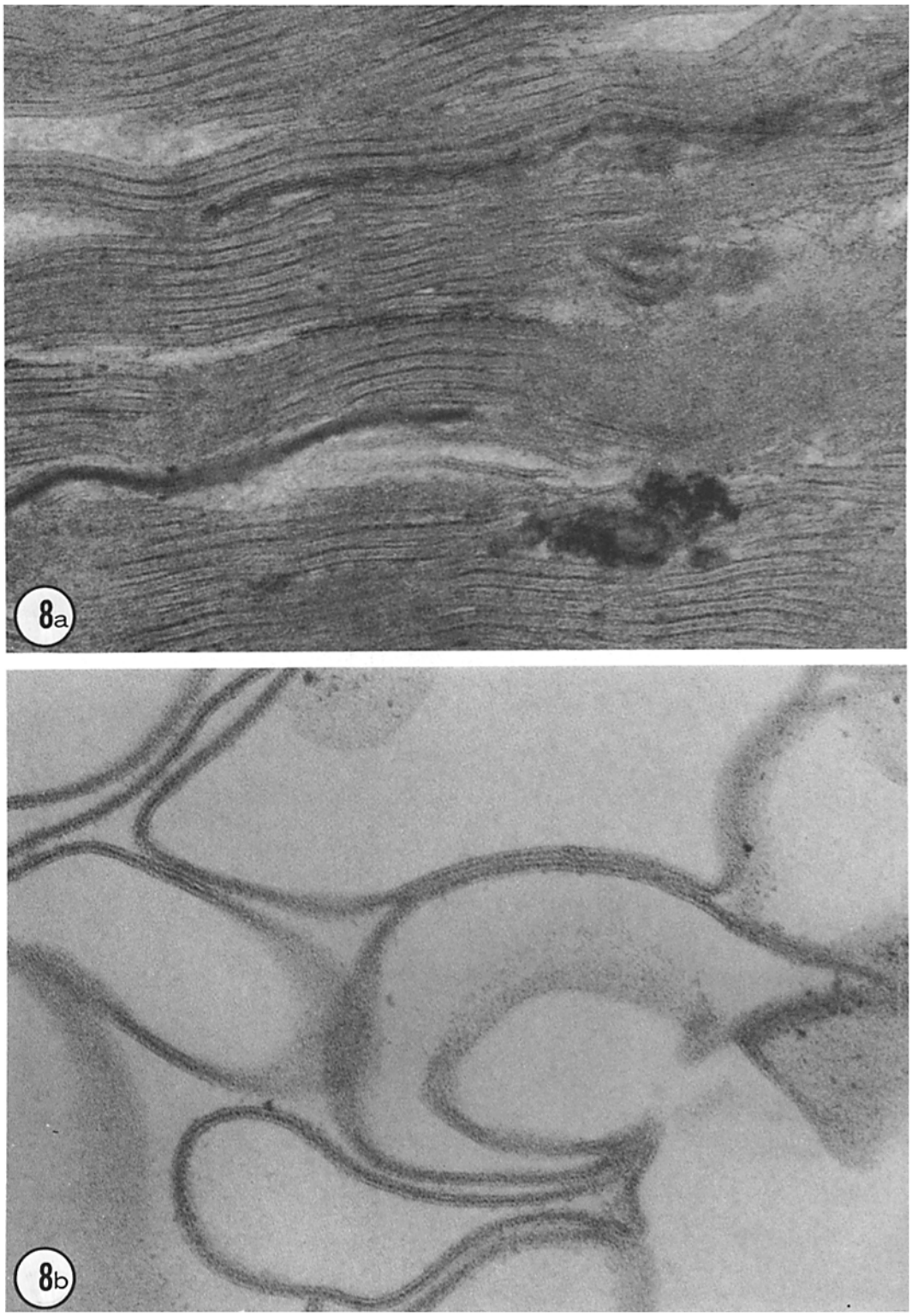

FIGURE 8 Electron micrographs of thin sections of junction pellets (*a*) (× 140,000) partially dried and (*b*) (× 140,000) treated with trypsin. The specimen in (*a*) was prepared like that in Fig. 7*b* but was then partially dehydrated by equilibrating through the vapor phase with a 1 M sucrose solution. The dehydration leads to regular stacking of the junction layers with some regions of disorder where the junctions are curved. Trypsin treatment of the junctions induces them to form closed vesicles. Centrifugation does not flatten the vesicles, and produces little orientation in the pellet. Close packing of junction pairs similar to that seen in Fig. 7*b* does occur where the vesicles are in contact with each other.

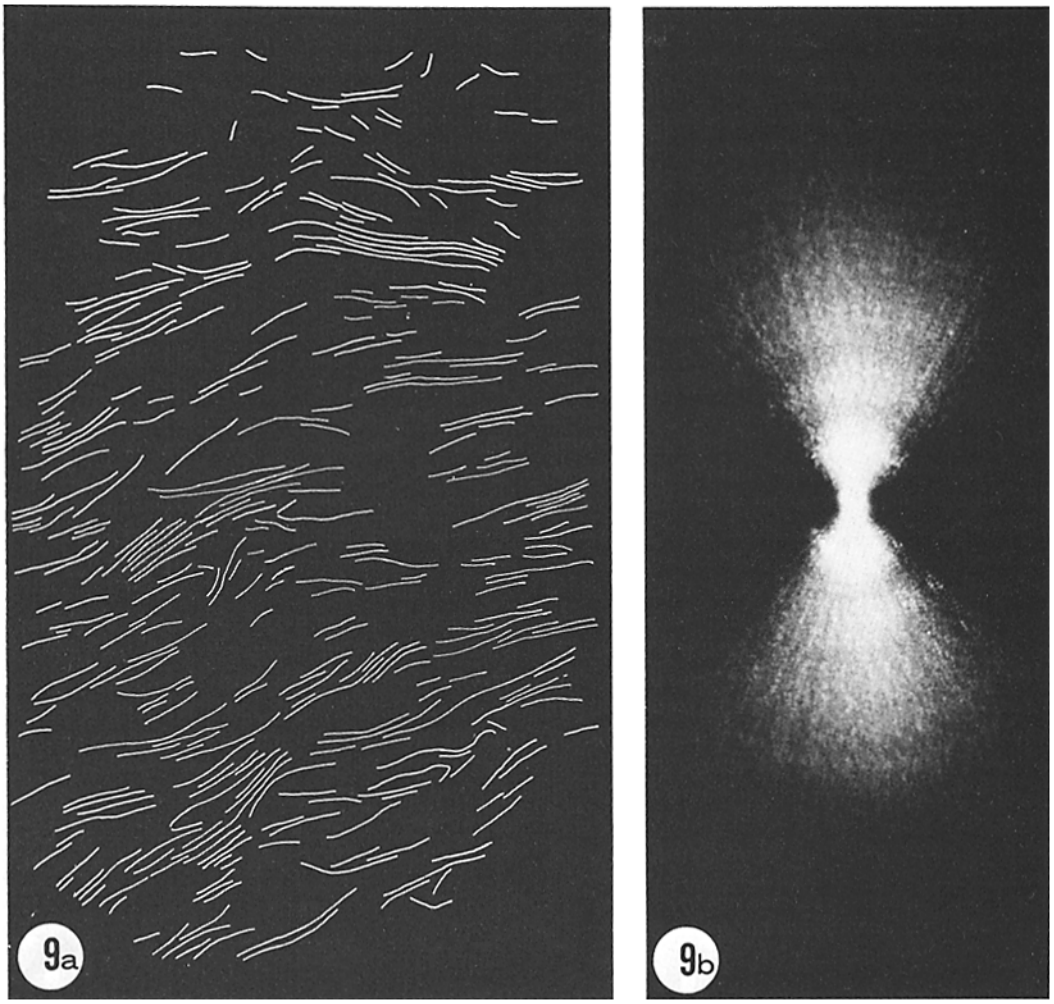

FIGURE 9 A tracing (*a*) from a micrograph of a thin section of a junction pellet similar to that shown in Fig. 7*b*, with its optical transform (*b*). The interference fringes due to partial ordering of the junctions are visible in the optical transform. The fading of the transform at higher angles is due to the finite thickness of the lines in the tracing. In overexposed optical diffraction patterns, at least eight or nine interference fringes are visible. The period of the fringes corresponds to a spacing of about 150 Å which is the separation of the closest packed junctions in the centrifuge pellet.

peak at 40 Å spacing. Figure 11*d* shows a diffraction pattern from a fresh, unfixed specimen. This pattern is very similar to patterns from specimens fixed in glutaraldehyde. The diffraction patterns from unfixed specimens tend to deteriorate with time over a period of days, whereas fixed specimens were stable over many months' storage at 4°C.

Biochemical Data

Gap junctions purified by treatment with collagenase and hyaluronidase appear to be composed of one principal protein, connexin, with a mol wt of about 20,000 daltons as measured by polyacrylamide gel electrophoresis in sodium dodecyl sulfate (SDS). This protein can be reduced to a lower mol wt of approx. 10,000 daltons by treatment of the SDS-dissolved samples with disulfide reducing agents (11, 12, 13). While precautions are taken to avoid proteolysis, it is likely that the junction proteins have been enzymatically cleaved during the isolation procedure. Proteolysis is unlikely to cleave those portions of the molecule embedded in the lipid bilayer or spanning the gap,

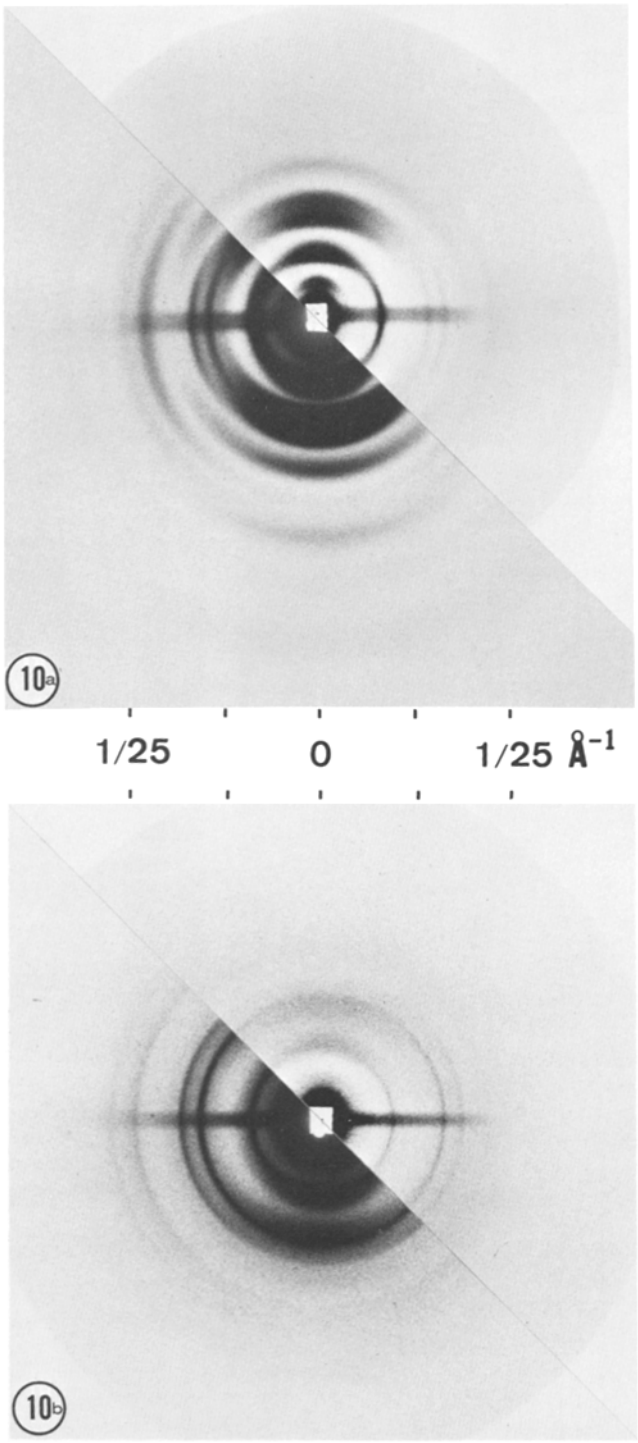

FIGURE 10 X-ray diffraction patterns from isolated gap junctions. The diffraction pattern in (*a*) is from specimen E153, a glutaraldehyde-fixed specimen similar to the one shown in thin section in Fig. 7*b*. The meridional diffraction extending vertically from the center of the pattern is determined by the electron density distribution perpendicular to the plane of the junction. The set of sharp arcs on the equator of the photograph are hexagonal lattice reflections corresponding to a lattice constant of 86.7 Å. The equatorial X-ray reflections from the hexagonal lattice viewed edge-on correspond to the spots in the optical diffraction from micrographs of the lattice viewed face-on (cf. Fig. 2). The horizontal streak is due to parasitic scatter from the monochromator. (*b*) Diffraction pattern from a trypsin-treated specimen (F38) fixed in glutaraldehyde. The poor orientation is caused by the formation of vesicles as shown in the micrograph in Fig. 8*b*. The equatorial reflections are sharper than in (*a*) and index to a lattice constant of 82 Å, which is nearly 5 Å less than that of specimen E153. The meridional diffraction is weaker relative to the equatorial than in the diffraction from specimen E153. Differences in the relative strengths of meridional and equatorial diffraction are correlated with differences in the lattic constant of specimens.

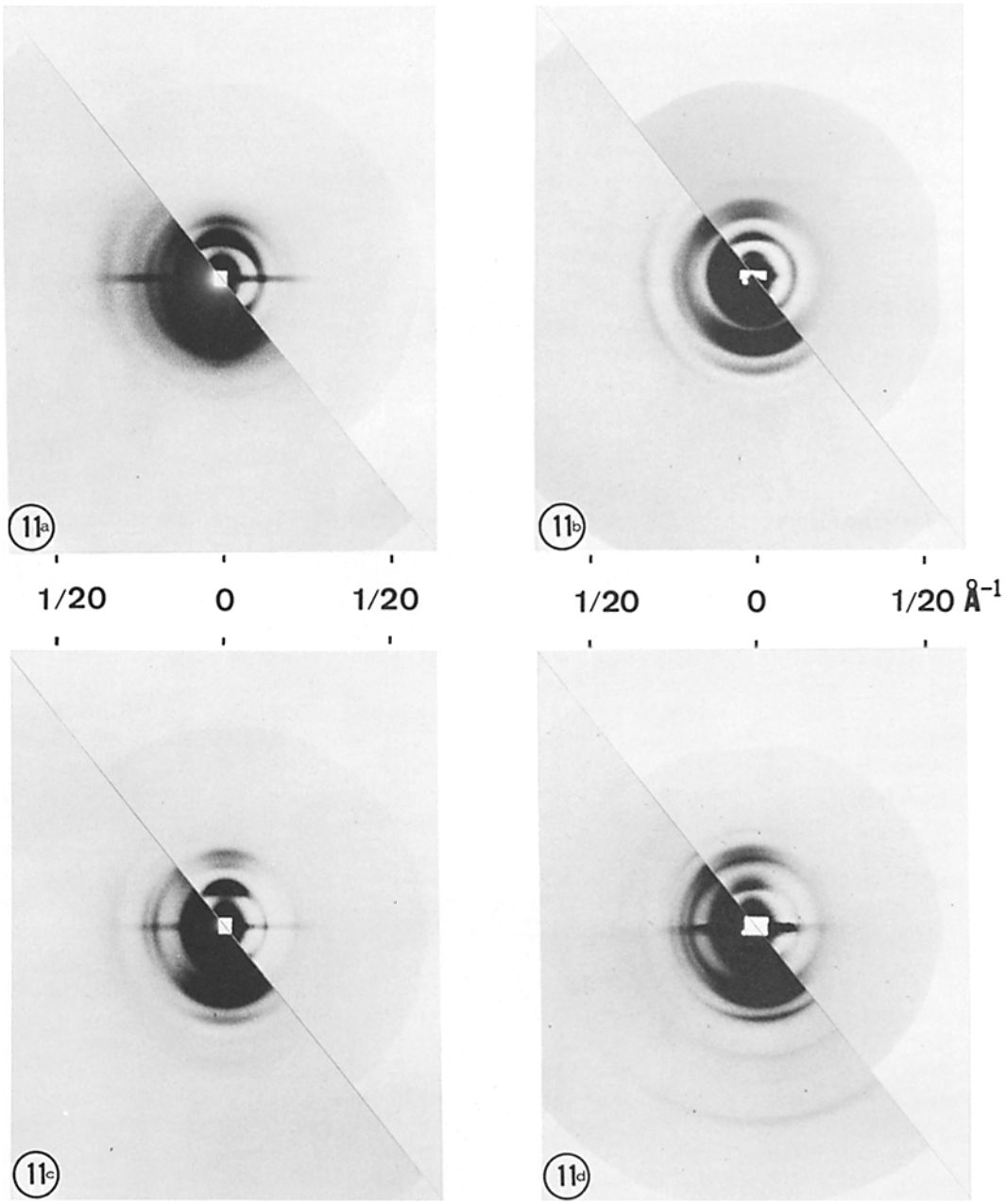

FIGURE 11 X-ray diffraction patterns from isolated gap junctions. (*a*) A diffraction pattern from the same specimen (E153) used to obtain the diffraction pattern in Fig. 10 after the specimen was dried in air. The low-angle diffuse scatter increased significantly on drying, and the intensity of the hexagonal lattice reflections decreased. The lattice constant decreased only by about 0.5 Å on drying. (*b*) A diffraction pattern from a different pellet of specimen E153 to which Hg had been added. There were no distinctive changes in the intensity distribution in the pattern which could be attributed to specifically bound Hg. The lattice constant measured from this photograph was 88.0 Å. (*c*) X-ray diffraction pattern from a partially dehydrated specimen (F68A). A micrograph of a thin section of this specimen is shown in Fig. 8*c*. The partial drying increased the orientation and ordering of the specimen but did not increase the low-angle diffuse scatter as the air drying did in (*a*). The lattice constant of this specimen was 85.7 Å. (*d*) X-ray diffraction pattern from an unfixed specimen (F6). The intensity distribution is very similar to the patterns from specimens fixed in glutaraldehyde. The life-time of unfixed specimens was much shorter than that of the fixed specimens. The lattice constant of this specimen was 84.1 Å.

TABLE I

Meridional and Equatorial Diffraction Spacings of Selected Gap Junction Specimens

Specimen	Comments	Meridonal zeros*			Lattice constant‡
			$Å^{-1}$		Å
E153	Glutaraldehyde fixed	0.0102	0.01730	0.02741	86.7
E153	+Hg	0.0098	0.01672	0.02704	88.0
E153	Dehydrated	0.00874	0.01753	0.02762	86.1
F38	Trypsin	0.0116	0.01931	0.03002	82.0
F22A	Trypsin (1st measurement)	0.01187	0.01852	–	83.6
F22A	Trypsin (2nd measurement) (6 days after the first)	–	0.01899	0.0304	82.8
F22A	Trypsin (3rd measurement) (27 days after the second)	0.01211	0.01904	–	81.2
F6	Unfixed	0.01006	0.01818	0.02835	84.1

* Positions of the low-angle minima in the meridional diffraction.

‡ Lattice constants measured from the positions of the equatorial diffraction maxima.

but the exposed portions of the protein on the cytoplasmic side of the junction could be susceptible to cleavage. Any proteolysis which occurs during junction isolation does not destroy gap junction structure as visualized by X-ray diffraction and by electron microscopy. The trypsin treatment, when used in the isolation procedure, does not significantly affect the buoyant density of the junction as shown in Fig. 12. Further, no additional cleavage of junction protein by the trypsin treatment is detected in SDS gels.

Thin-layer chromatography of chloroform-methanol extracts of the junctions reveals several phospholipids. The neutral lipid fraction which accounts for 10–20% of the junction lipids consists mainly of cholesterol. A more detailed analysis of the lipid and protein composition is now being undertaken.

The nitrogen and phosphorus content of whole junctions was determined by Galbraith Laboratories. The chemical analysis of specimens shows that the junctions contain 8% nitrogen by weight and 1.9% phosphorus by weight. Amino acid analyses attempted thus far have revealed no phosphorylated amino acids. Thus, all junction phosphorus can be assumed to be lipid phosphorus. With this assumption, the N/P ratio can be used to estimate the protein and lipid content of the junction.

Assuming an average mol wt of 700 for the phospholipids, the phosphorus, which has a mol wt of 31, will be 4.4% of the total phospholipid weight, indicating that phospholipids make up about 43% of the junction weight. Adding to this the estimated neutral lipid content, the junction contains 47–52% lipid by weight. Assuming 1 mol of nitrogen/mol of phospholipid, 2% of the phospholipid weight or 0.9% of the junction weight will be lipid nitrogen. Since the junction is 8% nitrogen by weight, it must contain 7.1% protein nitrogen by weight. From amino acid analyses of the junctions, the protein is found to be approx. 15.7% nitrogen. Therefore, the protein makes up about 46% of the total junction weight. The protein and lipid content estimated from the nitrogen and phosphorus content of the specimens accounts for more than 90% of the junction weight. The missing 2–7% is an indication of the uncertainty in the measurements. Furthermore, electron micrographs often suggest that there is some nonjunctional membrane in these preparations. Within the uncertainties of the chemical analysis and of the specimen purity, there are approximately equal weights of lipid and protein in the junctions.

The buoyant density of the junctions was measured by centrifugation on a continuous sucrose gradient. The results of these experiments are shown in Fig. 12. The buoyant density of the junctions measured in this fashion was 1.17 and did not change significantly with trypsin treatment. Comparisons of this buoyant density with that of other membrane preparations where the proportion of protein and lipid has been determined indicate that there are approximately equal weights of protein and lipid in these junction specimens. For instance, the buoyant density in sucrose of erythrocyte ghosts which are approx. 50% protein and 50% lipid by weight is also 1.17 (1, 19).

DISCUSSION

In the introductory paragraphs, we posed two questions about the junction structure: Do the connexons really form tubes that link the proto-

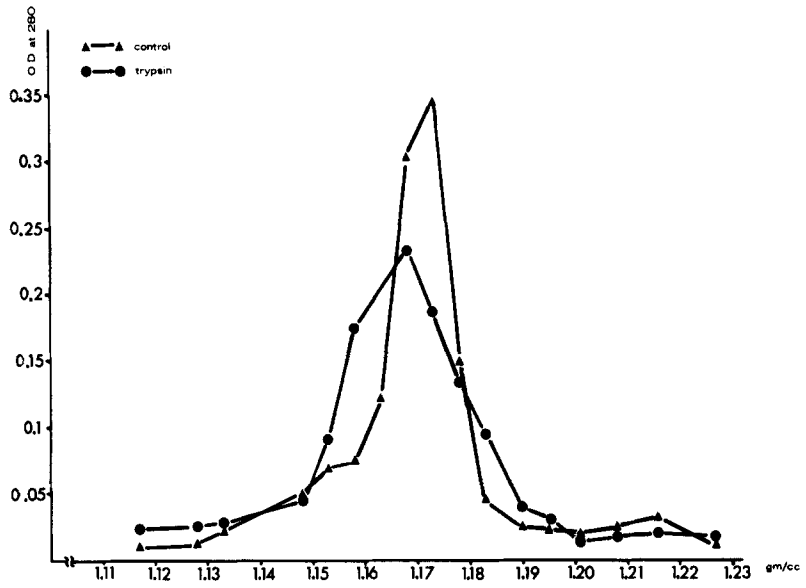

FIGURE 12 Buoyant density of isolated gap junctions and isolated gap junctions treated with trypsin. Absorption at 280 nm was measured for aliquots of junctions centrifuged in a continuous sucrose gradient. The peak position did not change significantly with trypsin treatment.

plasms of the connected cells? And what sort of interactions hold the connexons together in the junction lattice? An answer to the first question is provided by the molecular model for the junction based on measurements of diffracted X-ray intensities formulated in the following paper. Its resolution is low since the disorder in the structure limits the detail that can be seen both from the X-ray diffraction patterns and from the electron micrographs. In view of the results on the lattice variation and disorder presented in this paper, the second question can be rephrased: What sort of interactions can maintain such regular hexagonal long-range order but at the same time allow such large short-range disorder? More information about intermolecular forces than is provided by analysis of connexon packing arrangements would be required for a complete answer to this question; but analysis of the disordered packing does help to relate the lattice symmetry to the underlying molecular interactions.

Variations in Lattice Dimensions

Table I lists a sampling of the lattice dimensions observed by X-ray diffraction. The observed spacings range from 81 to 88 Å. The lattice constant of one specimen decreased by about 2 Å over a period of about a month. Smaller lattice constants were often observed in those specimens which had the additional treatment with trypsin compared to those treated only with collagenase and hyaluronidase. However, no strong correlations can yet be made between conditions of specimen preparation and lattice constant since the variation in lattice constant among specimens prepared in similar ways is comparable to the difference in the average lattice constant between groups.

Lattice constants measured from electron micrographs of negatively stained gap junctions varied over a similar range, the largest measured being about 10% greater than the smallest. Micrographs of negatively stained junctions also show the coexistence of domains with measurably different lattice constants, such as in Fig. 5. A range of lattice constants will broaden the observed equatorial reflections in the X-ray patterns. Most of the X-ray photographs in Figs. 10 and 11 have relatively broad reflections, suggesting inhomogeneity of lattice constants within the specimens. Occasionally, as in the diffraction pattern from F38 shown in Fig. 10*b*, the observed equatorial reflections are very sharp.

In some specimens, pairs of hexagonal reflections were observed corresponding to lattices with two distinct lattice constants. These two lattice structures appeared to be localized in different portions of the centrifuge pellet, since, in one diffraction pattern from these pellets, only a single

set of lattice reflections was present. The inhomogeneous character of these pellets demonstrates the difficulties in producing specimens with the same lattice constant.

Both X-ray diffraction and electron microscope data indicate that a change in the connexon structure may be associated with the variation in lattice constant. The data in Table I show that the positions of the minima of the meridional diffraction change with lattice constant, and that, as the lattice constant decreases, these minima move to larger diffraction angles. A comparison of the reconstructed images of negatively stained gap junctions in Fig. 3 shows that the distribution of stain in gap junctions may also be different in specimens with different lattice constants.

LATTICE DISORDER: Disorder in the packing of connexons can be analyzed directly from electron micrographs as was done in Fig. 4 or indirectly through its effect on the optical diffraction from micrographs as in Fig. 5. In negatively stained preparations of isolated gap junctions, the connexons pack with considerable local disorder while maintaining long-range order in large lattice domains which often occupy a substantial portion of the isolated junction plaque. Sharp diffraction peaks are observed in the optical diffraction patterns from these micrographs because of the long-range order. The short-range disorder reduces the intensity of the higher-order reflections, and the degree of disorder determines the number of observable diffraction peaks. To obtain a quantitative measure of lattice disorder, the connexon centers were marked in Fig. 5, and an optical transform was taken of the array of dots marking the connexon positions. This process insured that other effects such as the Fourier transform of the unit cell and defocusing effects (9) did not interfere with the analysis of disorder.

X-ray diffraction patterns are affected by disorder in much the same way as the optical diffraction patterns from electron micrographs. The effect of short-range disorder is to lower the diffracted intensities of the higher-angle reflections. The X-ray diffraction patterns almost always show a (2,0) reflection if any equatorial diffraction is apparent. In most patterns, the (2,1) is visible, and the (3,0) can be seen on a significant fraction of these patterns. These data indicate an average lattice order in the X-ray specimens similar to that seen from optical diffraction of electron micrographs of individual junctions. In some X-ray diffraction patterns the (4,0) reflection can be seen. The (4,0) reflection is the highest-order reflection which can be seen in optical diffraction patterns from the most highly ordered, negatively stained gap junctions.

Widths of X-ray reflections are determined by several factors. As shown in Fig. 5, different lattice constants give rise to diffraction at different radii in an optical diffraction pattern. This effect will broaden the equatorial lattice reflections of the X-ray patterns. However, the presence of off-equatorial diffraction coupled with poor orientation complicates any estimate of the range of lattice constant or the degree of long-range order from the widths of the X-ray reflections. Small domain size also broadens the widths of crystalline diffraction maxima. Examination of many micrographs indicates that single crystalline domains are extensive, usually fifty to several hundred unit cells on a side, so that broadening due to small domain size is likely to be insignificant compared to other contributions. However, the lattice domains may be distorted. The lattice is occasionally bent, and the lattice constant may vary from place to place within the domain. These distortions have the effect of increasing the width of the X-ray reflections.

In micrographs of freeze-fractured gap junctions from whole mouse liver, the lattice is usually poorly ordered. The array often appears liquid-like rather than crystalline. The P-face usually shows significantly less order than the E-face, indicating that at least some of the disorder is due to plastic deformation. However, fracture faces from livers perfused with hypertonic sucrose show considerably better ordering on both P- and E-faces. Perrachia (20, 21) has observed that treatments which uncouple junctional communications lead to a decrease in lattice constant and an increase in order. These results suggest that the connexons may be relatively disordered in vivo and that the isolation procedure has the effect of ordering the units into a more regular array.

Because we have electron microscope images in which the disorder in gap junctions can be observed, a model for the disorder can be constructed that allows simple conclusions to be made about the forces holding the junction lattice together. This model building procedure is less abstract and perhaps more informative than the statistical treatments used in the study of liquids or disordered arrays for which only X-ray diffraction data are available.

Figure 12 shows two model lattices and their

optical diffraction patterns. The well-ordered lattice, Fig. 13*a*, is regularly hexagonal, and its optical transform, Fig. 13*c*, exhibits sharp reflections which extend to high angles, fading only because of the finite size of the dots in the model lattice. The poorly ordered lattice, Fig. 13*b*, is a photograph of a model where the units were restricted to circles which were placed on an exact hexagonal lattice. The diameter of the circles was equal to one-third the lattice constant. Thus, the model exhibits short-range disorder similar to that observed in the gap junctions. At small diffraction angles, its optical diffraction pattern, Fig. 13*d*, is dominated by discrete reflections. At higher angles, the intensities of the sharp reflections diminish and they disappear into the diffuse scattering arising from the short-range disorder. The fall-off of the intensities of the discrete reflections in the diffraction pattern from this disordered array is very similar to that seen in optical diffraction from negatively stained gap junctions and that seen in the X-ray diffraction from gap junctions. Beyond the (4, 0) reflection, the diffuse scattering is about as strong as the lattice reflections. Thus, the disorder in gap junctions must be similar to that in the model. This means that the maximum displacement of the connexons from the regular hexagonal lattice points is about 15 Å in the best-ordered specimens.

LATTICE SYMMETRY AND MOLECULAR INTERACTIONS: The connexon as seen in electron micrographs has a diameter of about 60 Å with a 20 Å diameter pore through the center. The volume of a 75 Å-long cylindrical tube with these radial dimensions is about 190,000 Å^3. A protein structure occupying this volume and having the amino acid composition as measured for isolated gap junctions would have a mol wt of about 150,000 daltons. It would take four to eight copies of a protein of mol wt 20–30,000 to occupy this volume. If there is an appreciable amount of protein extending on the cytoplasmic side of the membrane, the molecular weight estimated for the connexon would be larger. The mol wt of the protein subunit as measured on SDS gels for junction preparations treated with proteolytic enzymes is about 20,000. This component may correspond to the portion of the junction protein subunit that spans the membrane bilayer of the junction.

To maintain long-range order in the hexagonal lattice, each unit must have six nearest neighbors; and although the separation between nearest neighbors can vary over relatively large distances, each unit seems constrained to stay within some limiting distance of its ideal equilibrium lattice position. This regularity suggests some specificity in the interactions that maintain the sixfold coordination.

It is possible that the arrangement is maintained by nondirectional long-range forces, as in swollen gels of tobacco mosaic virus (6), but the combination of long-range order with short-range disorder does suggest some directional specificity that keeps each unit in contact with its six neighbors. Without a directionality in the interactions consistent with the lattice symmetry, the high degree of short-range disorder would seem more likely to give rise to a liquid-like packing than to the large single crystalline domains observed. Since the number of protein subunits estimated from the protein molecular weight and morphology is in the range of 4–8, it is most likely that the connexon is a hexamer.

Electron microscope observations show that the connexons are connected in pairs across the gap. If the two units in a pair are identical, as they appear to be, then they must be related by a twofold axis parallel to the plane of the junction at the center of the gap. If the individual connexon has sixfold rotational symmetry and the pair are connected with their sixfold axes coincident, the assembly will have point group symmetry 622, which has six twofold axes perpendicular to the sixfold axis. Arranging the units in a hexagonal lattice so that the twofold axes line up will generate a layer with the symmetry of the space group P622, which has P6m symmetry in projection. The morphological observations indicate that the junction may, in fact, have this symmetry.

The symmetry is only exact when the junctions are flat. Usually, however, the junctions are curved and the paired connexons can then only be related by local twofold axes. The curvature can be accounted for by different lattice constants on the two sides of the structure. The smallest radius of curvature observed is for the double walled vesicles of trypsin-treated specimens and is of the order of 1,500 Å. Since the thickness of the junction is about 150 Å, a radius of curvature of 1,500 Å corresponds to a difference of 10% in the distance between the connexons on the two cytoplasmic surfaces. This variation of lattice constant is well within the range of variations observed in different specimens.

COMPARISON OF X-RAY AND ELECTRON MICROSCOPE RESULTS: A significant result of

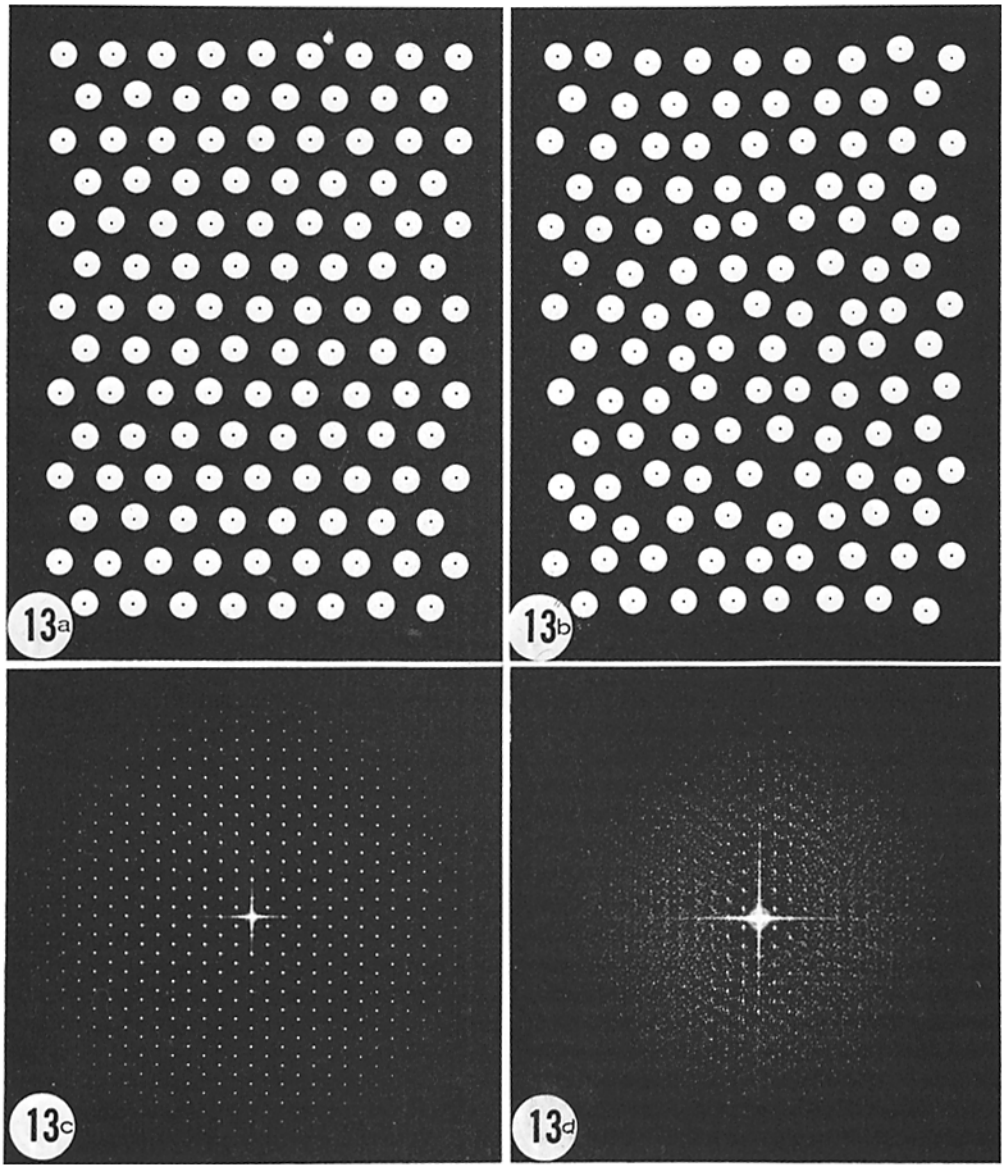

FIGURE 13 Model illustrating the effect of short-range disorder on the optical diffraction pattern. The model was constructed from a sheet of lucite by drilling a hexagonal array of holes 1/4 inch in diameter with a lattice constant of 3/4 inch. A thumbtack was placed in each hole. The ordered array in (*a*) was produced by placing the tacks in equivalent positions in each hole. The disordered array in (*b*) was produced by randomly displacing the tacks in the holes. The dimensions of the holes allow a variation in position which is $\pm 1/6$ of the lattice constant so that separation of neighboring units can vary by up to $\pm 1/3$ the lattice constant. Dots were marked at the center of each tack in photographs of the arrays, and optical diffraction patterns were taken from the array of dots. The optical diffraction patterns represent the Fourier transform of the arrangement of units. This is similar to the procedure used to optically analyze the arrangement of units in the micrograph in Fig. 5. The diffraction pattern (*c*) from the well-ordered lattice in (*a*) shows sharp diffraction spots out to the limit set by the size of the dots marking the positions of the units. In the diffraction from the disordered array in (*d*), the intensity of the sharp reflections fades out rapidly with increasing diffraction order. Beyond the fourth order, the intensity of the sharp reflections is comparable to that of the diffuse diffraction from the disordered array. The disorder is greater in the horizontal than in the vertical direction, producing an asymmetry in both the diffuse scatter and the fade-out of sharp reflections. The displacement of the units in (*b*) from their equilibrium positions is random, but long-range order is maintained as indicated by the sharpness of the spots in the diffraction pattern. The optical analysis shows that the disorder in this array is comparable to that seen in micrographs of the junction lattices.

these studies is the very close correspondence between the data from X-ray diffraction and from electron microscopy. The disorder in the junction lattice and the lamellar stacking in the centrifuge pellets as measured by these two methods are virtually identical. The observable hexagonal lattice reflections in optical diffraction patterns from electron micrographs of negatively stained specimens extend to about the same Bragg spacing as those in the X-ray diffraction patterns from hydrated junctions. This indicates that no gross changes in the lattice packing are produced by the preparation of negatively stained specimens. The correspondence of the junction stacking measured from X-ray patterns and from micrographs of thin sections obtained from the same specimens has been useful in the quantitative analysis of the junction electron density profile (18).

Coordinated use of electron microscopy and X-ray diffraction is more informative than applying each method independently. Micrographs of periodic macromolecular assemblies can be used to directly phase X-ray diffraction patterns if the regular structure is preserved in the microscope (7, 17). Conversely, X-ray diffraction patterns of native, hydrated specimens can be used to judge how well the structure is preserved in the electron microscope. Using the micrographs for detailed interpretation of the diffraction patterns requires, of course, well-preserved specimens. Measurement of the disorder in gap junctions by X-ray diffraction and electron microscopy of corresponding specimens has provided a sensitive test of structure preservation. The disorder in X-ray specimens prepared in different ways can vary widely, indicating that the arrangement of the units reflects a delicate balance of forces; the fact that the same arrangements can be preserved in electron microscope specimens suggests that the structure of the structural units is also reasonably well preserved. The electron microscope images of the gap junction structure can therefore be used (18) for interpretation of the X-ray patterns.

We would like to thank W. Saunders for assistance with the photography, D. Paul and C. Ingersoll for technical assistance, and Dr. N. B. Gilula for providing the micrograph analyzed in Fig. 2.

This work was supported by National Institutes of Health grant no. CA15468 (D. L. D. Caspar), National Science Foundation grant no. PCM7409713 (D. L. D. Caspar and D. A. Goodenough), National Institutes of Health grant no. GM18974 (D. A. Goodenough) and American Heart Association grant no. 73707 (D. A. Goodenough). L. Makowski was supported by a National Institutes of Health traineeship from National Institutes of Health grant no. GM01555 to the Department of Electrical Engineering, Massachusetts Institute of Technology.

Received for publication 21 May 1976, and in revised form 18 April 1977.

REFERENCES

1. Barclay, M., R. K. Barclay, E. S. Essner, V. P. Skipski, and O. Terebus-Kekish. 1967. Plasma membranes of rat liver: Isolation of lipoprotein macromolecules. *Science (Wash. D. C.)* **156:**665-667.
2. Benedetti, E. L., and P. Emmelot. 1965. Electron microscope observations on negatively stained plasma membranes isolated from rat liver. *J. Cell Biol.* **26:**299-305.
3. Benedetti, E. L., and P. Emmelot. 1968. Hexagonal array of subunits in tight junctions separated from isolated rat liver plasma membranes. *J. Cell Biol.* **38:**15-24.
4. Benedetti, E. L., and P. Emmelot. 1968. Structure and function of plasma membranes isolated from liver. *In* The Membranes. A. J. Dalton and T. Haguenau, editors. Academic Press, Inc., New York. 33-120.
5. Bennett, M. V. L. 1973. Function of electrotonic junctions in embryonic and adult tissues. *Fed. Proc.* **32:**65-75.
6. Bernal, J. D., and I. Fankuchen. 1941. X-ray and crystallographic studies of plant virus preparations. *J. Gen. Physiol.* **25:**111-146.
7. Caspar, D. L. D., C. Cohen, and W. Longley. 1969. Tropomyosin: crystal structure, polymorphism and molecular interactions. *J. Mol. Biol.* **41:**87-101.
8. Dunia, J., C. S. Ghosh, E. L. Benedetti, A. Zweens, and H. Bloemendal. 1974. Isolation and protein pattern of eye lens fiber junctions. *FEBS (Fed. Eur. Biochem. Soc.) Lett.* **45:**139-144.
9. Erickson, H. P., and A. Klug. 1971. Measurement and compensation of defocusing and aberrations by Fourier processing of electron micrographs. *Phil. Trans. R. Soc. Lond. B. Biol. Sci.* **261B:**105-118.
10. Gilula, N. B. 1974. Isolation of rat liver gap junctions and characterization of the polypeptides. *J. Cell Biol.* **63**(2, Pt. 2):111*a*. (Abstr.).
11. Goodenough, D. A. 1974. Bulk isolation of mouse hepatocyte gap junctions. *J. Cell Biol.* **61:**557-563.
12. Goodenough, D. A. 1975. Methods for the isolation and structural characterization of hepatocyte gap junctions. *In* Methods in Membrane Biology. Vol. III. E. D. Korn, editor. Plenum Publishing Corp., New York.
13. Goodenough, D. A. 1976. *In vitro* formation of

gap junction vesicles. *J. Cell Biol.* **68**:220–231.
14. GOODENOUGH, D. A., and N. B. GILULA. 1974. The splitting of hepatocyte gap junctions and zonulae occludentes with hypertonic disaccharides. *J. Cell Biol.* **61**:575–590.
15. GOODENOUGH, D. A., and J. P. REVEL. 1970. A fine structural analysis of intercellular junctions in mouse liver. *J. Cell Biol.* **45**:272–290.
16. GOODENOUGH, D. A., and W. STOECKENIUS. 1972. The isolation of mouse hepatocyte gap junctions. *J. Cell Biol.* **54**:646–656.
17. JACK, A., S. C. HARRISON, and R. A. CROWTHER. 1975. Structure of bushy stunt virus. II. Comparison of results obtained by electron microscopy and X-ray diffraction. *J. Mol. Biol.* **97**:163–172.
18. MAKOWSKI, L., D. L. D. CASPAR, W. C. PHILLIPS, and D. A. GOODENOUGH. 1977. Gap junction structures. II. Analysis of the X-ray diffraction data. **74**:629–645.
19. MITCHELL, C. D., and D. J. HANAHAN. 1966. Solubilization of certain proteins from the human erythrocyte stroma. *Biochemistry.* **5**:51–57.
20. PERACCHIA, C., and A. F. DULHUNTY. 1976. Low resistance junctions in crayfish. Structural changes with functional uncoupling. *J. Cell Biol.* **70**: 419–439.
21. PERACCHIA, C. 1977. Gap junctions. Structural changes after uncoupling procedures. *J. Cell Biol.* **72**:628–641.
22. REVEL, J. P., and J. J. KARNOVSKY. 1967. Hexagonal array of subunits in intercellular junctions of the mouse heart and liver. *J. Cell Biol.* **33**:C7–C12.
23. ROBERTSON, J. D. 1963. The occurrence of a subunit pattern in the unit membrane of club ending in Mauthner cell synapses in goldfish brains. *J. Cell Biol.* **19**:201–221.